Embryonic development of the shell in *Biomphalaria glabrata* (Say)

ULRICH BIELEFELD* and WILHELM BECKER

Zoologisches Institut und Zoologisches Museum, Hamburg, Germany

ABSTRACT **During embryogenesis of the fresh water snail *Biomphalaria glabrata* (Say) (Pulmonata, Basommatophora) shell formation has been studied by light and electron microscopical techniques. The shell field invagination (SFI), the secretion of the first shell layers, the development of the shell-forming mantle edge gland and spindle formation have been investigated. During embryonic development at 28°C environmental temperature, the shell field invaginates after 35 h. After 40 h the SFI is closed apically by cellular protrusions and scale-like precursors of the periostracum. The first electron translucent layer of the periostracum stems from electron dense vesicles of the cells which lie at the opening of the SFI. A second electron dense layer appears some hours afterwards. When the shell appears birefringent in the polarizing microscope (45 h of development) calcium can be detected in it using energy dispersive x-ray analysis. As calcification occurs the intercrystalline matrix appears under the periostracum and the SFI begins to open. In embryos of 60 h the mantle cavity appears at the left caudal side. When the mantle edge groove develops (65 h of development) lamellate units are added to the outer layer of the periostracum, but no distinct lamellar layer is formed in *B. glabrata*. In addition to the lamellar cell and the periostracum cell, a secretory cell can be observed in the developing groove. After 65 h of development, spindle formation starts and the shell begins to coil in a left hand spiral. After 5 days of development the embryos are ready to leave the egg capsules.**

KEY WORDS: *development, gastropod, shell, ultrastructure, electron microscopy*

Introduction

Embryonic development of basommatophoran snails has attracted the interest of biologists ever since Rabl described the «Entwicklung der Tellerschnecke» (Planorbidae) over a hundred years ago, in 1879. Since then larval development of Planorbid snails has been investigated by Holmes (1900) for Planorbarius, Wierzejsky (1905) for Physa and others (Raven, 1966; Moor, 1983; Verdonk and Biggelaar, 1983). More recently Kawano and Simoes (1987) described the inductions of teratological alterations in the head organs of *Biomphalaria glabrata*. They based their study on the work of Camey and Verdonk (1970), who studied cell lines in early development. However, there is only one SEM study on the larval development of the basommatophoran *Lymnaea*, which was done by Morrill (1982).

This paper provides an Electron Microscopical (EM) description of shell morphogenesis during normal development of *B. glabrata*. For pulmonate snails, there are only EM studies on *Lymnaea* by Kniprath (1977) and more information is required «concerning how, when and where embryonic shell material is secreted» (Watabe, 1988). It is the aim of the present investigation to shed light on the functional analysis of tissue ultrastructure by correlating the appearance of new shell layers with the differentiation of the shell-forming tissue. Special emphasis is laid on investigating the role of the SFI, the function of which has been questioned recently again (Eyster, 1986).

Results

The trochophore larva at 35 h of development is spherical (Fig. 1A) and the prototroch encircles the larva on the left and right sides. The apical plate is free of cilia and densely covered by small microvilli. The cephalic plates can be distinguished from the other body surfaces by the spotted pattern of microvilli and the small size of the cells. In the dorsal region, the prototroch ends at the head vesicle and the somatic plate (Fig. 1B). The cells of the somatic plate bear microvilli only at their lateral cell borders but the head vesicle is covered with microvilli.

The prospective shell field can be identified first as a small indentation close to the borderline between head vesicle and somatic plate (Fig. 1B). At this site, the cells of an area of 30 μm

*Address for reprints: Zoologisches Institut und Zoologisches Museum, Martin-Luther-King Platz 3, D-2000 Hamburg 13, Germany. FAX: 40-4123.3937
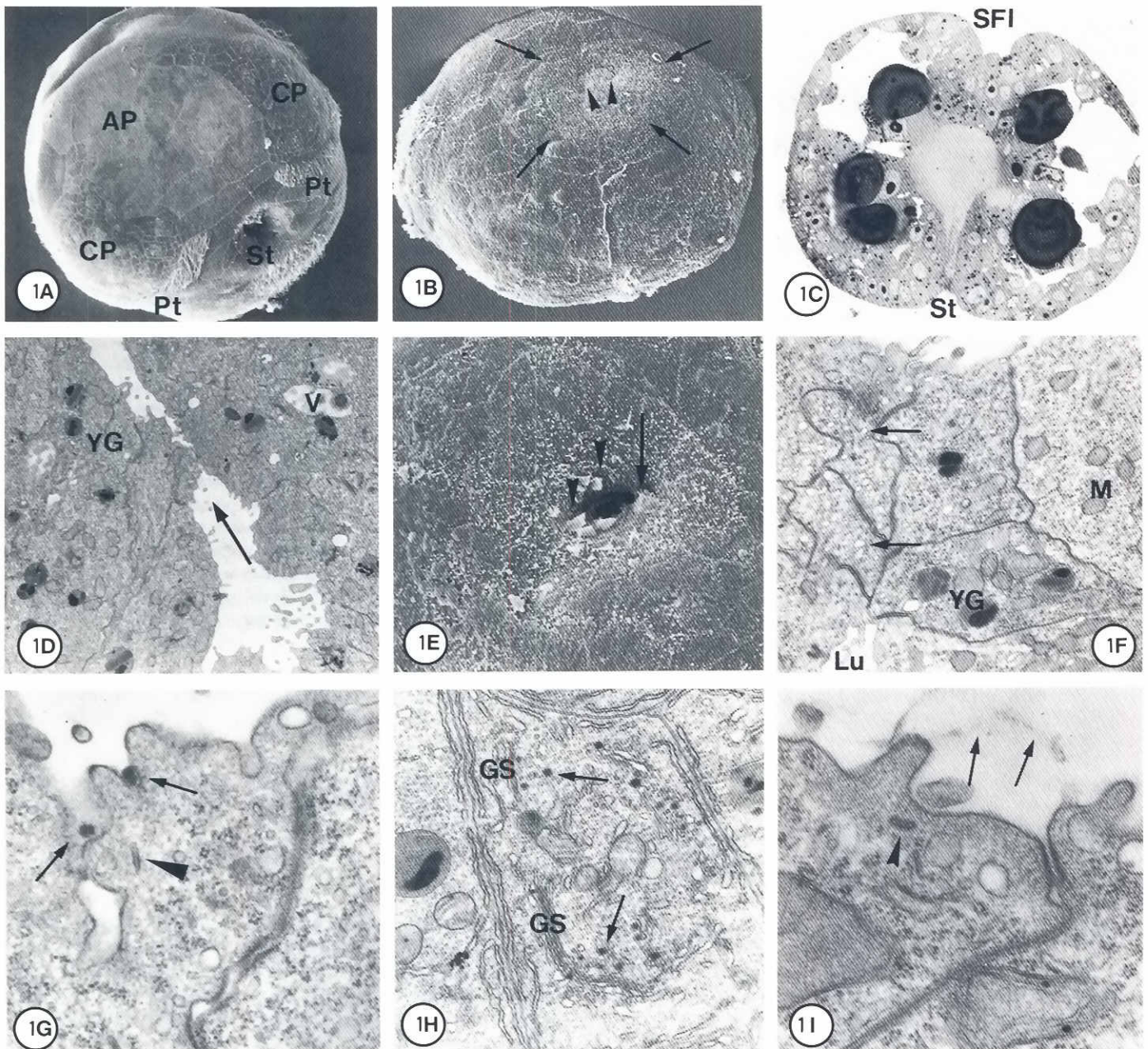
Fig. 1. The formation and closure of the SFI in trochophore larvae. A-C show trochophore larvae with 35 h of development. D-J stem from one batch of 37 h of development. *(A) SEM x350. Frontal view showing prototroch (Pt), stomodeum (St), apical plate (AP) and cephalic plates (CP).* **(B)** *SEM x500. Dorsal view. The site of the prospective shell field invagination has developed densely packed microvilli (arrows). The SFI seems to start as a curved furrow (arrowheads).* **(C)** *LM x350. Cross section in the frontal plane. Opposite to the ciliated stomodaeum (St) the SFI (SFI) appears.* **(D)** *TEM x3720. Apical protrusions (arrow) of the cells within the SFI contact the other side of the SFI. In the cytoplasm there are yolk granules (YG) and vacuoles (V) which are late stages of ectodermal albumen metabolism.* **(E)** *SEM x1500. Dorsal view showing cellular protrusions (arrow) and first shell material (arrowheads) at the rim of the closing SFI.* **(F)** *TEM x10600. Apices of SFI cells bridge the lumen (Lu). The cytoplasm contains mitochondria (M), yolk granules (YG) and electron lucent vesicles (arrows).* **(G)** *TEM x40300. Detail of a cell at the rim of the SFI. Electron-dense material is secreted (arrows) via long secretion channels. The arrowheads indicate narrow cisternae.* **(H)** *TEM x13800. Detail of acell at the rim of the SFI showing Golgi-stacks (GS) with electron-dense vesicles (arrows) at the trans-side.* **(I)** *TEM x32150. Fibrillous material (arrows) adheres to the top of SFI cells. Arrowhead indicates narrow cisternae.*

in diameter bear microvilli at their apex. In sections through this region, one can see that the endoderm opposite to the stomodaeum makes contact with the ectoderm (Fig. 1C). However, no ultrastructural indications for intercellular contacts could be observed. The ectodermal cells seem to be drawn into the body and the resulting indentation is called Shell Field Invagination (SFI).
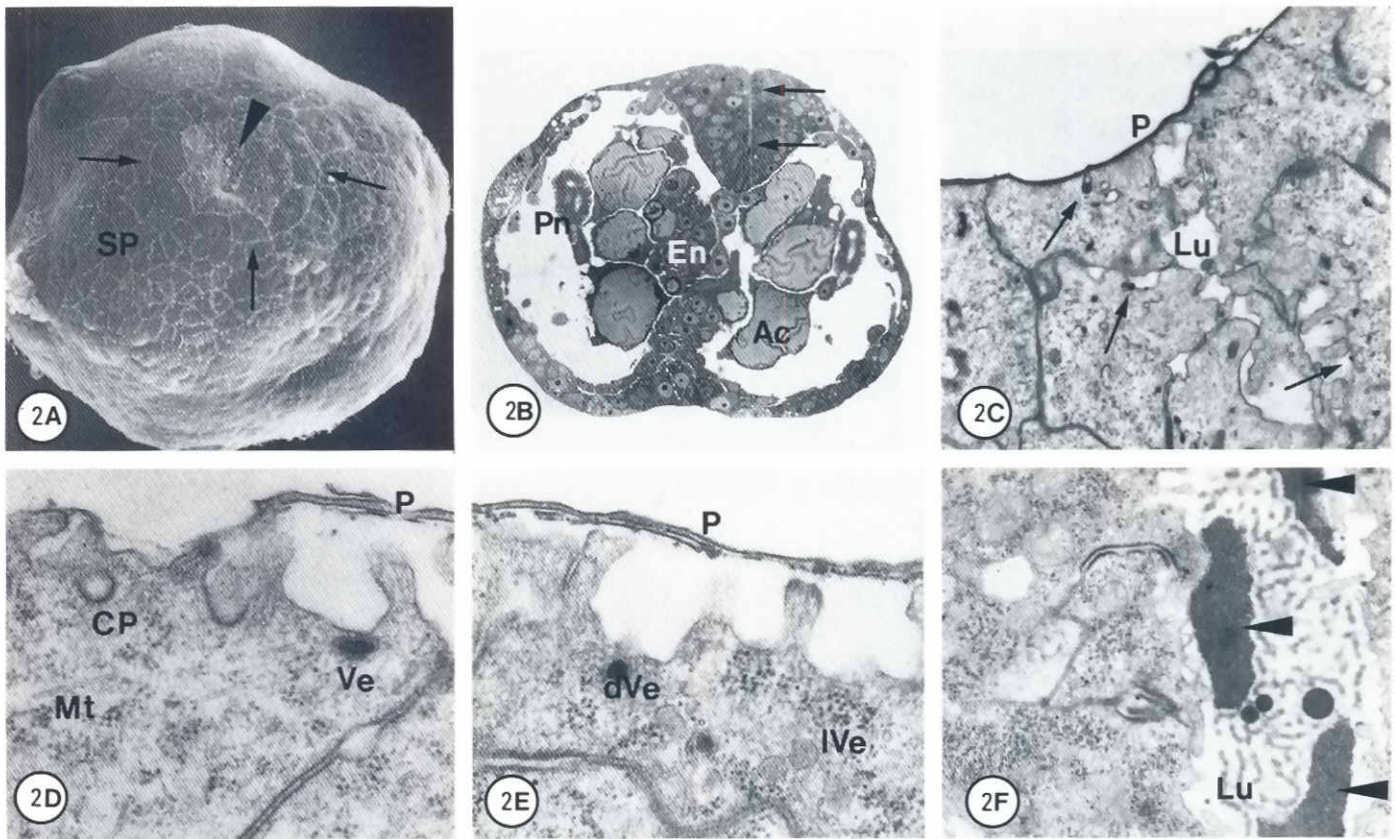
Fig. 2. The formation of the periostracum in trochophore stage (37-40 h). The TEM specimens were fixed according to Probst (1986). **(A)** *SEM x500. Cells, of which the microvilli form a rosette-like structure (arrows), enclose the SFI, which is covered by the periostracum (arrowhead).* **(B)** *LM x300. Cross section of the apical part of the SFI, which is a narrow channel of about 50 μm (arrows). Albumen storing endodermal cells (Ac), small endodermal cells (En) and the pair of protonephridia (Pn) fill the body.* **(C)** *TEM x11870. Lateral cross section through the central opening of the SFI. The SFI is closed by the periostracum (P). Electron dense vesicles (arrows) are secreted into the apical SFI lumen (Lu) and directly onto the periostracum.* **(D)** *TEM x44540. Apex of periostracum-secreting cells at the lateral side of the shell field. Electron-dense vesicles (Ve), coated pit (Cp) and microtubules (Mt) are visible. The first fibrillous strand of the first layer of the periostracum (P) rests on top of the microvilli.* **(E)** *TEM x45730. Electron-dense (dVE) and electron-lucent vesicles (lVe) add the next fibrillous strand to the outer layer of the periostracum (P).* **(F)** *TEM x15610. Electron-dense fine granulate material (arrowheads) can be found in the basal lumen (Lu) of the SFI.*

The SFI becomes deeper and cellular projections protrude at its rim (Fig. 1D). In these cells no ultrastructural indications for the start of shell formation can be found. Compared to other ectodermal cells, the cells of the SFI have more Golgi-stacks and more large vacuoles, which are intermediate stages in albumen or yolk degradation. The SFI is closed apically by cellular protrusions and first shell material (Fig. 1E). The apices of the cells which bridge the lumen of the SFI are filled with numerous electron lucent vesicles (Fig. 1F). Other cells secrete apically the electron dense content of vesicles (Fig. 1G) which are produced by the Golgi-apparatus in the perinuclear region of the cells (Fig. 1H). Apically, small cisternae lie in the cells at the rim of the SFI (Fig. 1G and 1I). On top of the microvilli of those cells which border the rim of the SFI (Fig 1I) a fine fuzzy line appears which probably is the first material for the embryonic periostracum.

In embryos of 40 h of development, a small indentation which is covered by shell material indicates the closed invagination (Fig. 2A). The cells in the periphery of the shell field bear microvilli only at their apical cell borders. Therefore, the shell field is surrounded by a rosette-like ring of microvilli. The SFI is a narrow channel of about 50 μm (Fig. 2B) and it is sealed apically by the periostracum (Fig. 2C). In the centre of the shell field, the periostracum rests on smooth apices of cells and the electron dense content of vesicles is extruded via narrow channels. Electron dense vesicles can also be observed between the intermingled microvilli and cell apices of the outer third of the SFI. These vesicles seem to pass through the narrow lumen of the SFI to the central part of the shell. Laterally the periostracum rests on microvilli. Furthermore there are coated pits at the apical membrane. (Fig. 2D). Numerous microtubules probably mediate the intracellular vesicle transport. In specimens which were fixed according to Probst (1986) the periostracum consists of fibrillous strands of 25nm thickness. These strands seem to be put together in one layer with an increasing thickness towards the centre (Fig. 2E). In the basal part of the SFI, there is electron dense material. Due to its fine granular ultrastructure (Fig. 2F) it is considered to be albumen.
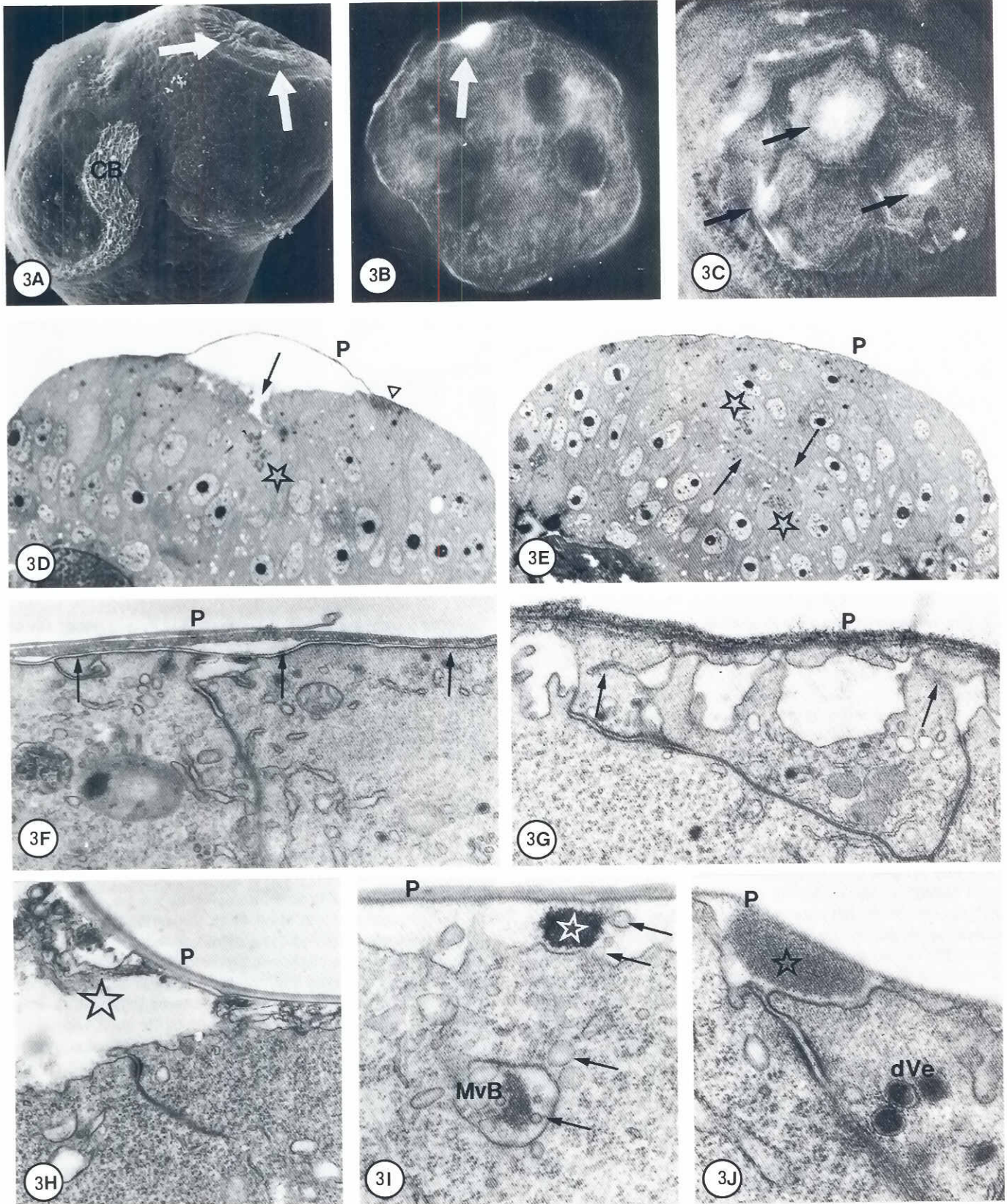
After 45-50 h of development, when the shell field has a diameter of about 80-90 µm (Fig. 3A), the centre of the shell detaches from the underlying tissue and forms a cup. In this stage, birefringence of the shell can be observed in the polarizing microscope (Fig. 3B). Birefringence is due to calcification because calcium can be detected with energy dispersive X-ray analysis (Graph A). Only in specimens which are fixed according to Probst (1986) are the minerals retained, and they are not homogeneously but patchily distributed in the shell (Fig. 3C).

Under the shell, the SFI pore widens (Fig. 3D and E). Numerous mitotic stages indicate rapid growth of the SFI epithelium. Cells revealing microvilli at their apices secrete the outer layer of the periostracum in vesicles of varying electron density as shown in Figs. 2D and E. Towards the centre of the shell field the cells have a smooth apex and the shell material is secreted via narrow channels (Fig. 3F). At this site, a fine electron line appears under the outer layer of the periostracum. Where the periostracum detaches from the tissue, the apical parts of the cells seem to be ripped off as they are separated from the cell basis by invagination of the lateral cell membrane (Fig. 3G). The septate junctions are located below this perforated cell apex. The ripped off apices dissolve in the extrapallial space (Fig 3H).

Material of the intercrystalline matrix appears under the periostracum. In decalcified specimens this material is extremely osmiophilic and accumulates below the inner electron dense layer of the periostracum (Fig. 3I). At the apex of the underlying cells, slightly oval vesicles are shed between the microvilli. These vesicles seem to stem from multivesicular bodies which contain fuzzy material. In contrast to the intercrystalline matrix, the periostracal material exhibits medium electron density (Fig. 3J).

Embryos with 50-55 h of development have a calcified shell with a diameter of more than 130 µm and cilia tufts surround the shell field margin (Fig. 4A). The SFI is evaginated (Fig. 4B). After 60 h, a histological zonation can be observed in the mantle edge gland: the groove begins to sink into the connective tissue, the high columnar epithelium of the belt and the low columnar epithelium of the outer mantle epithelium (OME) differentiate (Fig. 4C).

In the developing OME the site of synthesis of the intercrystalline matrix could not be identified more precisely, as indicated in Fig. 3J. In addition to the vesicles, which can be found at the apex, vacuoles of 0.5-1µm lie in the supernuclear region of the cells. The vacuoles contain fibrillous material in varying forms (Fig. 4D) and Golgi-vesicles fuse with them. Accumulations of granules of strong electron density can be found in the intercellular spaces (Figs. 4D-
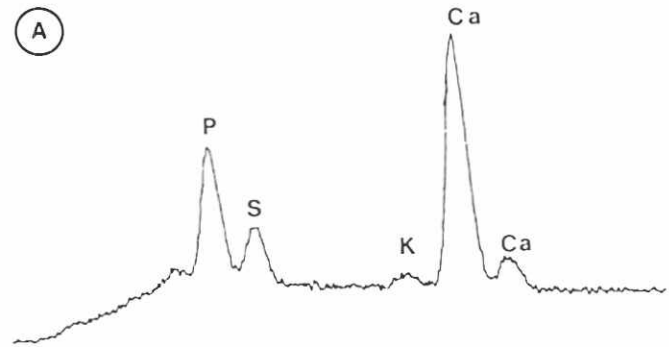
Graph A. **Patterns of energy dispersive X-ray microanalysis of shells** *which were recorded under the following conditions: the probe was set at an angle of 45° at a distance of 29mm, recording time 100 sec, counting rate 1000 counts/sec, magnification x3000. Embryo of 45- 50 h as shown in Fig. 3C. Analysis of the bright spots in the shell induces distinct calcium peaks (Ca). Potassium (K), phosphorous (P) and sulfur (S).*

E). Once the embryos are older than 90 h of development a new cell type which is filled with secretory granules appears in the OME (Fig. 4F). In embryos with more than 65 h of development at least three cell types can be observed at the basis of the groove (Fig. 5A). The periostracum-forming cells are filled with vesicular rER (Fig. 5B). Distally located to the periostracum-forming cells, a lamellar cell can be observed. Apically it extrudes units of 250 nm length and 2 nm thickness (Fig 5A), which are added to the outer layer of the periostracum. In cross section the units appear hollow; two thin lines are separated by an electron translucent space and every unit is enclosed in a membrane compartment. In the perinuclear region, the membrane compartments including this unit appear at the trans-site of the Golgi-stacks (Fig. 5C). The membrane compartments can fuse to form vacuoles of 0.7µm in diameter filled with densely packed units (Fig. 5D). Distally located to the lamellar cell, a third cell type can be distinguished, which is filled with electron-dense vesicles of 150-200 nm (Fig. 5A). In this cell type, the rER appears in small strands and the Golgi-apparatus is well developed (Fig. 5E). In embryos with 90 h of development, the mantle edge gland has fully differentiated above the pulmonary cavity (Fig. 5F). Sections of the gland in which the shell is attached to the tissue help to identify

Fig. 3. **Calcification of the embryonic shell in trochophore stage with 45 h of development. (A)** *SEM x400. Dorso-lateral view showing the shell (arrows) and the ciliary band (CB) of the former prototroch.* **(B)** *Polarizing LM x200. The shell (arrow) is birefringent. The whole-mount specimen was fixed in buffered paraformalin some minutes before the picture was taken.* **(C)** *SEM x630. Dorsal view showing the shell of an embryo, which was fixed for SEM according to Probst (1986). The X-ray analysis (shown in Graph A) revealed calcium only in the bright spots (arrows). The resolution of the SEM is diminished due to carbon coating and a reduced sensitivity of the probe.* **(D and E)** *LM x850. Consecutive semithin sections through the SFI. The periostracum (P) has detached centrally, where the SFI begins to open. The lumen is indicated by arrows. The invaginated epithelium grows by mitotic divisions (stars).* **(F)** *TEM x19760. Detail of the flat apex of the shell-forming cells. The site of the shell field is indicated with a triangle in Fig. 3D. An electron-dense line (arrows) can be observed underneath the outer layer of the periostracum (P).* **(G)** *TEM x21375. The apex of the cells seems to be ripped off when the periostracum (P) detaches from the tissue. The apex is separated from the cells by lateral invaginations (arrrows).* **(H)** *TEM x51330. The cellular material (star) is dissolved in the space between the periostracum (P) and the tissue.* **(I)** *TEM x40000. Under the periostracum, strongly electron-dense material (star) indicates the intercrystalline matrix. The cells secrete small vesicles (arrows), which seem to stem from multivesicular bodies (MvB).* **(J)** *TEM x39350. At the lateral end of the periostracum (P), its material which stems from electron-dense vesicles (dVe) might accumulate on top of the cells. It is not as dense as the material of the intercrystalline matrix.*
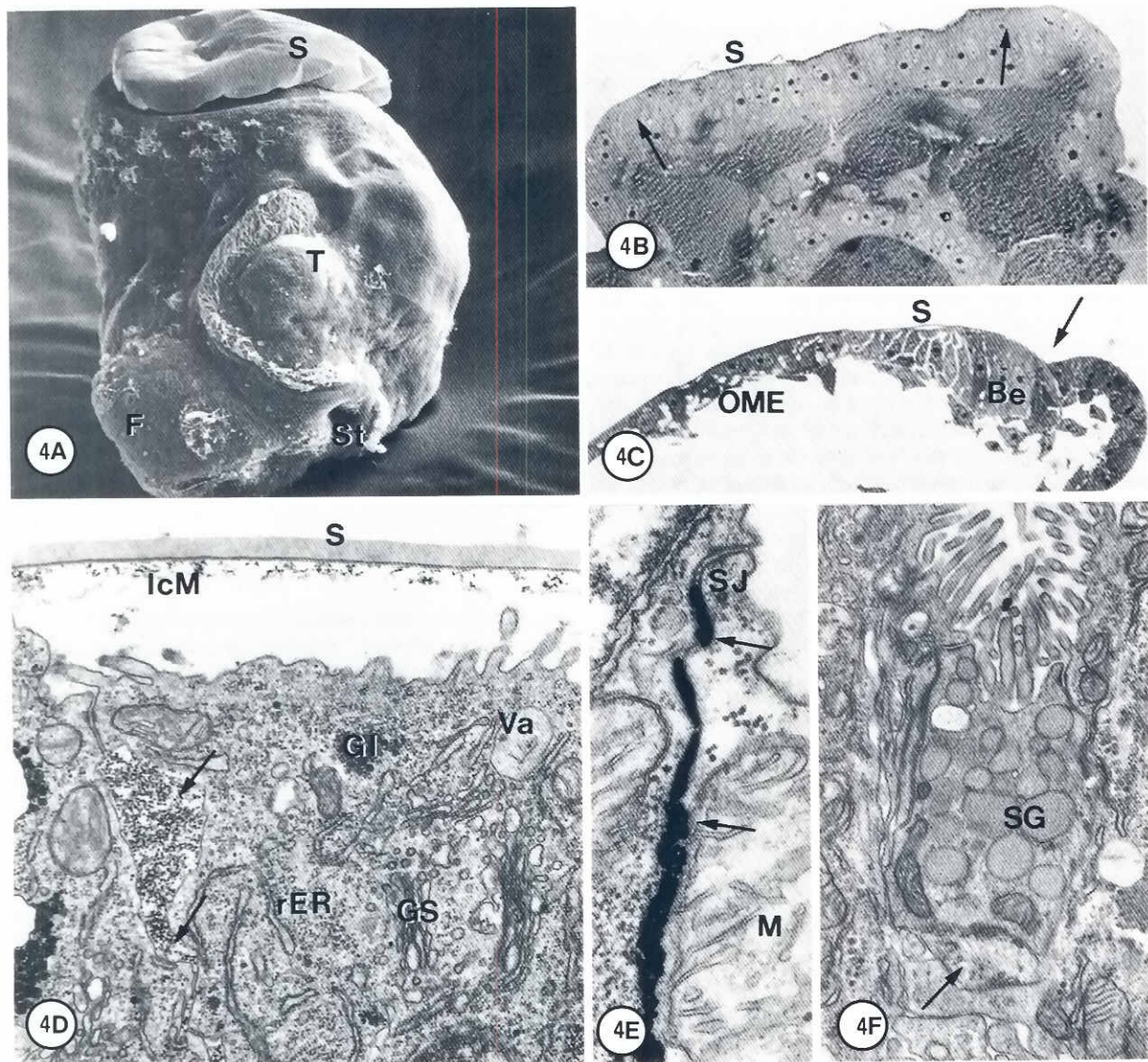
Fig. 4. The differentiation of the outer mantle epithelium. (A) *SEM x300. Lateral view showing the right side of an embryo after 50 h of development. The shell (S), tentacles (T), foot (F) and the stomodaeum (St) are distinct.* **(B)** *LM x520. Veliger stage (50 h). Cross section in the sagittal plane. The SFI has evaginated and the shell field is flat. The decalcified shell is attached laterally to the shell field margin (arrows), centrally it is loose.* **(C)** *LM x400. Veliger stage with 60 h of development. A zonation can be discerned between the low columnar cells of the outer mantle epithelium (OME) and the high columnar cells of the belt (Be). A small indentation (arrow) indicates where the groove develops.* **(D)** *TEM x11140. The cells of the OME have developed strands of the rER (rER) parallel to the lateral cell membrane. Numerous Golgi-stacks (GS) are associated with vacuoles (Va) of 0,5 μm. The content of the vacuoles often is fibrillous. Glycogen or galactogen (Gl) is accumulated. Electron-dense granules are found in the wide intercellular spaces (arrows). The decalcified shell (S) shows the intercrystalline matrix (IcM).* **(E)** *TEM x50814. The electron-dense material (arrows) might accumulate in the intercellular space up to the septate junctions (SJ). Mitochondrium (M).* **(F)** *TEM x16890. Late veliger stage with 90 h of development. A cell appears in the OME, that contains secretory granules (SG). Under the cell, a dendrit can be observed (arrow).*

the sites where the different layers of the shell are formed. The outer layer of the periostracum is formed at the basis of the fold and by the high columnar cells of the belt which bear microvilli at their apex. The dark layer of the periostracum is secreted in the distal part of the belt where the cells often have a smooth apex. The crystalline layer of the shell is secreted by the cells of the transient zone between the belt and the OME (Fig. 5G).

Fractured shells (Fig. 5H) exhibit one cross lamellar layer of crystals in the shell. In sections of decalcified shells the periostracum consists of three layers without a distinct lamellar layer. The electron-dense intercrystalline matrix consists of hollow envelopes which are aligned in one direction, indicating the cross lamellar orientation of the crystals (Fig. 5I). At the inner side of the decalcified shells the hypostracum appears as a layer of little

electron density. Spindle formation starts after 65 h of development, when the calcified shell covers the dorsal part of the embryo and the pulmonary cavity is a small indentation on the left side. At the right side of the embryos a tissue fold starts to grow bearing shell-secreting cells. With 80 h of development, the pulmonary cavity extends from the after to the rectal ridge (Fig. 6A). The protrusion has grown so long that it covers on the right side the old shell (Fig. 6B-C). Following the growth of the protrusion, the periostracum has formed first a hook and then the spindle. The embryos have about 90 h of development when the new shell material is attached onto the other shell (Fig. 6D-E). Initially, the periostracum material is secreted as vesicles (Fig. 6F) and the lamellar cell cannot be found in the shell-secreting tissue before the embryos have 90 h of development. After 5 days of development the embryos are ready to leave the egg capsules. At this stage, the diameter of the shells is about 600 μm.

Discussion

In all molluscan larvae, except those of the polyplacophorans, the shell field invaginates before the initial formation of the shell (Kniprath, 1981). For basommatophoran snails, there are three models of the histology and development of the SFI which are based on studies of embryos of *Lymnaea* (Raven, 1952, 1966; Timmermans, 1969; Kniprath, 1977) and the planorbid snail *Helisoma duryi eudiscus* (Kapur and Gibson, 1967). In general, our results for *Biomphalaria glabrata* can be compared to the model which has been described by Kniprath (1977, 1981) for *Lymnaea*, but ultrastructural details differ.

In the present investigation the site of SFI could be identified in the middle of the hypothetical prototrochal line extending to the dorsal half of the embryos. In fact this line is the border between the head vesicle and the somatic plate. Morrill (1982) in his Figs. 33A and 33B shows protruding cells in embryos of 20 and 36 h at the presumptive site for the shell field invagination. Similar structures could not be observed in *B. glabrata*.

Scale-like periostracum fragments and cellular protrusions are both involved in closing the invagination. In the SEM, the protrusions recall the lamellipodia which are reported for *Ilyanassa obsoleta* by Tomlinson (1987) and other gastropods by Eyster (1985, 1986). However, they differ in ultrastructure and function from the lamellipodia. Initial shell formation starts at the closing rim of the shell field invagination. Afterwards it is an organic layer on top of those cells that closes the SFI. In addition to the «rosette cells» which lie at the rim of the SFI, the cells that face the narrow porus also secrete shell material. Kniprath (1977) and Eyster (1983 in the opistobranch *Aeolidia papillosa)* report that the SFI is not involved in secretion of shell material.

Eyster (1986) pointed out that in at least three prosobranch and opistobranch species the SFI has a function in the calcification of the early shell. In *Lymnaea*, Kniprath (1977) reports calcification after the evagination of the SFI. Timmermans (1969) reported increased Ca^{45} incorporation in the embryonic shell of *Lymnaea* after the third day of development *i.e.* when the SFI evaginates. In *B. glabrata* the shell is birefringent when the SFI opens apically. The coincidence of these events rather supports a possible function of the SFI in calcification. Due to the formation of the SFI, the invaginated epithelium can continue to grow and to take up albumen from the SFI lumen. The albuminous fluid contains carbohydrates,

proteins and minerals such as calcium (Taylor, 1973). During and after evagination the cells might immediately participate in calcification of the shell because they lie underneath its center.

After the evagination of the SFI, the further differentiation of the mantle edge gland in *B. glabrata* follows histologically the model of *Lymnaea* as reported by Kniprath (1981). However, in *B. glabrata* initial shell formation and the ultrastructure of the differentiated shell differ from those observations reported for Lymnaea as shown in Fig. 3 by Kniprath (1981).

In the present investigation, the initially secreted layers of the embryonic shell are called periostracum because they strongly resemble those layers that can also be found in the periostracum of hatching embryos. In *Lymnaea*, lamellar units are postulated to form the first layer of the initially secreted periostracum. In *B. glabrata*, shell secretion starts with vesicles which form the first fibrillous strand of the periostracum. Very similar vesicles can also be found in the light and dark periostracum-secreting cells at the base of the mantle edge groove of the adults (Kniprath, 1972; Zylstra *et al.*, 1978; Saleuddin and Petit, 1983). In the embryos, several fibrillous strands are put together to increase the thickness of the outer layer of the periostracum. This layer resembles that shown by Jones and Saleuddin (1978) in the adult shells of *Physa*. An electron-dense layer of the periostracum is formed beneath the outer layer. From the first appearance onwards, cells with a smooth apex seem to be involved in its formation (Figs. 3F and 5F). Our studies of the late embryos showed that the inner layer of the periostracum is secreted at the second zone of the belt. Lamellar units which are described for all basommatophorans (Saleuddin and Petit, 1983) could not be observed before the groove is differentiated. No distinct lamellar layer occurs in the periostracum of *B. glabrata* even when the units are secreted. Instead, the lamellar units are blended into the outer layer of the periostracum.

In embryos with a birefringent shell, electron-dense material is observed under the periostracum. This material is extremely electron-dense due to the strong binding of uranyl acetate during «en bloc» staining, which indicates cation-binding structures (Goodford and Wolowyk, 1972). Therefore, it seems reasonable to consider this material as the intercrystalline matrix which should have strong affinity to cations (Wilbur and Saleuddin, 1983). In shell with a cross lamellar layer of crystals, the intercrystalline «envelopes» (Nakahara *et al.*, 1981) are also strongly electron dense. Furthermore, the hypostracum, which should not have affinity to cations, does not seem to be as electron dense as the envelopes.

In the fixed embryos of 45 h of development, the matrix is not homogeneously distributed but appears in clumps. This finding coincides with the heterogeneous distribution of the calcium in the shells of these embryos. Several attempts to detect calcium with the help of X-ray analysis in specimens fixed in a different way than ours failed. In fact our fixation is reported as a calcium precipitation method for transmission electron microscopy (Probst, 1986). Even in our specimens, calcium seems to be dislocated during fixation and further processing for electron microscopy. This might be related to the fact that initially the crystals are only weakly bound to the shell. Similar problems are reported by Eyster (1986) for marine prosobranch larvae.

The cells that synthesize the intercrystalline matrix should lie beside the cells secreting the periostracum. However, the ultrastructural site of synthesis for the intercrystalline matrix can only be speculated about. It could be secreted by small vesicles, as shown in Fig. 3I. They might contain the material for the intercrystalline
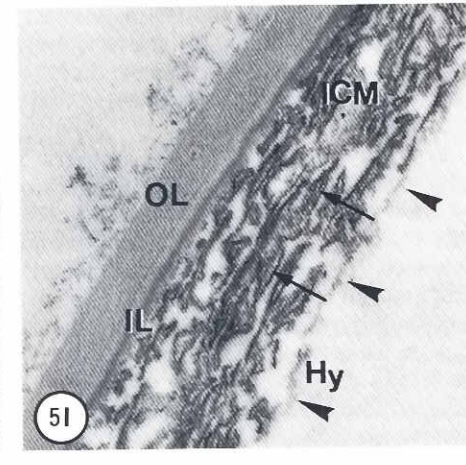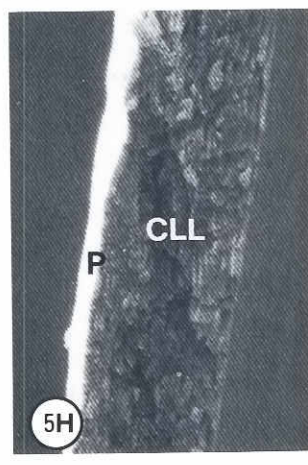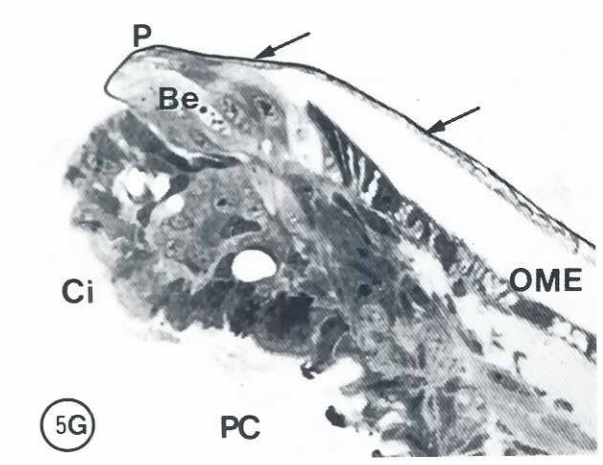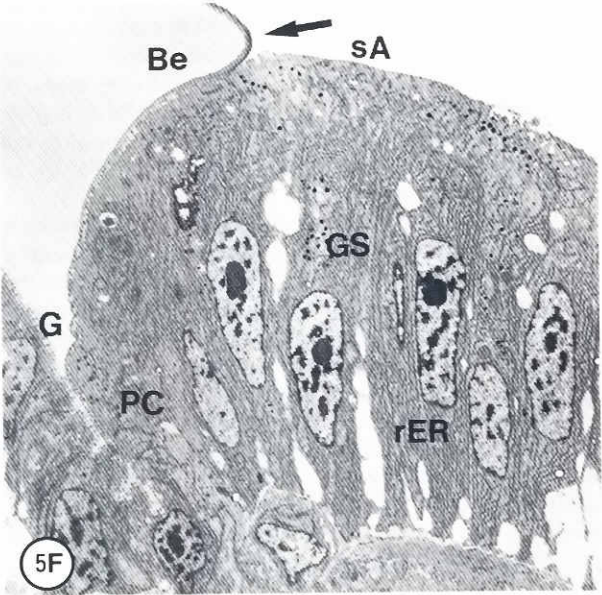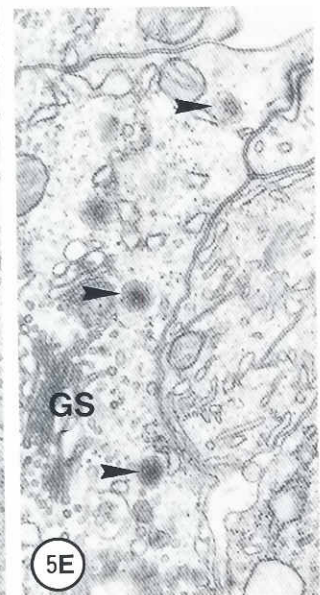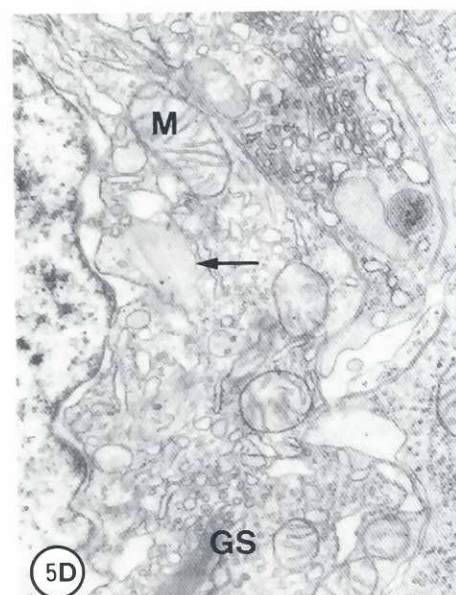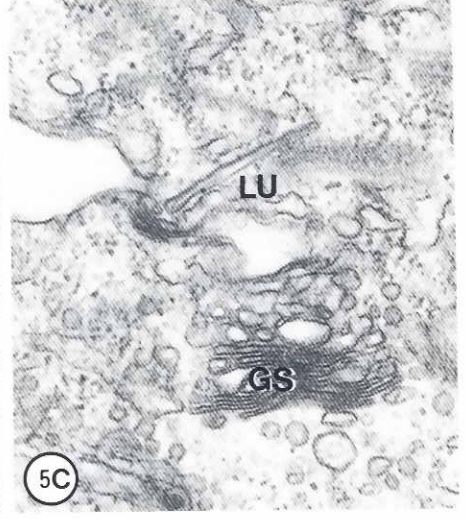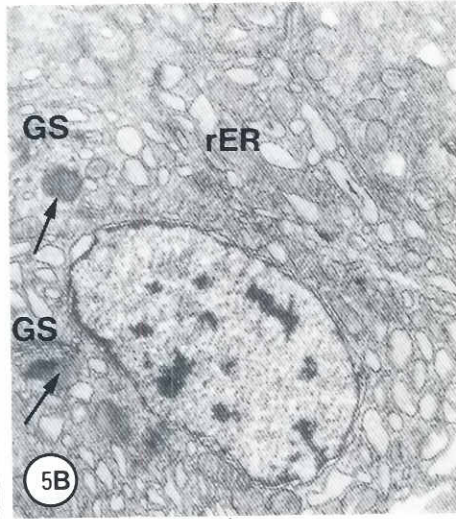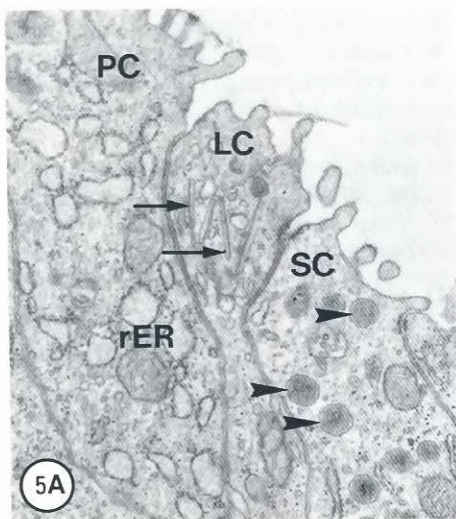
matrix which then has to be processed in the extrapallial space, to bind cations. Material, with strong cationic binding characteristics which appears in the widened intercellular spaces is considered as a calcium carrier of the hemolymph. Neff (1972) has reported the occurance of electron-dense granules in the outer mantle epithelium of *Mercenaria*. Similar granules could also be observed in our tissue.

It can be concluded that the secretory cell has no essential function in calcification because it appears when the shell already has a calcified layer. The cell very much resembles a mucous cell. A function of mucous in calcification has been reported by Humbert *et al.* (1989) in the intestine of eels. However, both Zylstra *et al.* (1978) and our own studies on adult tissue showed that the cell does not contain mucopolysaccharides and no calcium-binding substances (unpublished observations). Further studies should investigate the role of this cell type for shell formation. Our study of the late stages indicates that calcification begins in the transitional zone between the belt and the outer mantle epithelium (OME). This was postulated also by Boer and Witteveen (1980), who localized carbonic anhydrase in the transitional zone.

In the present investigation we were able to show that the layers of the shell that are located underneath each other are secreted one after the other following the closure of the SFI. Ultrastructurally there are no major differences between the early and the late tissue structures, which form the shell layers. These results are supported by the histochemical findings of Timmermans (1969) in embryos of *Lymnaea*. However, our EM study could cast new light on the function of the lamellar units which in *B. glabrata* seem to melt into the outer layer of the periostracum. Functions which were postulated for defined zones in the adult mantle edge gland (as reviewed by Saleuddin and Petit, 1983) could be corroborated. More information was obtained about the site of synthesis for the intercrystalline matrix and the role of the secretory cell in the OME.

More clearly than in previous papers based on light microscopy, the morphology of the larval stages could be demonstrated. For example, Camey and Verdonk (1970) report ciliary cells for the apical plate, which could not be observed in the SEM. In comparison to the time-tables of development reported for *Lymnaea* (Cumin, 1972) *B. glabrata* develops much faster even at 25°C. This capacity of fast development makes *B. glabrata* a convenient object for further developmental studies of all larval stages, which can be obtained within one week after egg deposition.

Materials and Methods

Adult *Biomphalaria glabrata*, Puerto Rico strain, were induced to lay eggs with a fresh-water stimulus (van der Steen, 1967). After the first cleavage, newly-laid egg masses were transferred to petri dishes with artificial soft water (28°C). After 30 h of development was completed, embryos were taken every five hours by carefully removing them from the egg capsules and rinsing them in water. For parallel investigations some specimens from the same batch were fixed for SEM and for TEM studies.

For SEM, first fixation was carried out for 2 h in 2% Glutaraldehyde (dissolved in phosphate buffer 0.01 M, pH 7.4). After rinsing in the same buffer, the embryos were postfixed in 1% osmium reduced by 1.5% bichromate (pH 7.5) (Probst 1986). Other specimens were fixed using cacodylic buffer (0.01 M, pH 7.4) and osmiumtetroxid (1% in the same buffer). The specimens were dehydrated in an ascending series of Ethanol, transfered stepwise to Freon 222 and critical point dried with liquid CO_2 as transition fluid. The embryos were glued with double sided tape on specimen holder stubs and spattered with gold for normal SEM. For energy dispersive X-ray microanalysis the specimens were coated with carbon. Investigations were performed with a Cambridge Stereoscan S4-10. X-ray analysis of the shells was done with an ORTEC SEM X-ray microanalyzing system. For the TEM investigation, other embryos from the same batch were fixed for 2 h in 2% Glutaraldehyde in 0.01 sodium cacodylate buffer, pH 7.4. After rinsing in buffer, the embryos were fixed in 1% osmium ferrocyanide for 2 h (Karnovsky 1961, McDonald 1984) and stained «en bloc» with 1% uranyl acetate in maleate buffer (pH 5.5). Some specimens were incubated over night in uranyl acetate (pH 5.5) for decalcification of the shell. After dehydration the specimens were embedded in Spurr's (Spurr, 1969) medium. Specimens shown in Fig. 2C-F were fixed according to Probst (1986). For TEM, ultrathin sections of 90 nm were cut with a diamond knife and counterstained with lead citrate (Reynolds, 1963). For LM, semithin sections of 1 μm thickness were stained according to Richardson *et al.* (1960).

References

BOER, H.H. and WITTEVEEN, J. (1980). Ultrastructural localization of carbonic anhydrase in tissues involved in shell formation and ionic regulation in the pond snail *Lymnaea stagnalis. Cell Tissue Res.* 209: 383-390.

CAMEY, T. and VERDONK, N.H. (1970). The early development of the snail *Biomphalaria glabrata* (Say) and the origin of the head organs. *Neth. J. Zool.* 20: 93-121.

Fig. 5. The cellular differentiation of mantle edge groove. (A) *TEM x19000. Veliger stage with 65-70 h of development. In the groove periostracum cells (PC) with dilated rER (rER), lamellar cells (LC) with lamellar units (arrows) and secretory cell (SC) with secretory granules (arrowheads) can be observed.* **(B)** *TEM x10000. The bases of the periostracum cells are sunken into the connective tissue. The cytoplasm is filled with dilated rER (rER) cisternae and vacuoles (arrows) of 500 nm, which are associated with the Golgi-stacks (GS).* **(C)** *TEM x46670. Detail of a lamellar cell. The lamellar units (Lu) are formed at the trans-site of the Golgi-stack (Gs).* **(D)** *TEM x17600. The perinuclear region of the lamellar cell is filled with mitochondria (M) Golgi-stacks (GS) and vacuoles (arrow) filled with lamella.* **(E)** *TEM x16630. A secretory cell with numerous Golgi-stacks (GS). The secretory vesicles (arrowheads) are about 200 nm in diameter.* **(F)** *TEM x2950. Cross section through the groove (G) and belt (Be) after 80 h of development. The overview shows the curled distal side of the groove, the cell necks of the periostracal cells (PC) and the cells of the belt with a height of 40μ. The cells of the belt are filled with rER (rER) strands and Golgi-stacks (GS) which produce electron-dense vesicles. The electron-dense inner layer (arrow) of the periostracum appears where the cell apices are smooth (sA).* **(G)** *LM x400. Cross section through the mantle edge gland after 80 h of development. The inner mantle epithelium with cilia (Ci) faces the pulmonary cavity (PC). The periostracum (P) can be observed in the groove, curving over the belt (Be). The calcified layer (arrows) can be observed first over transient zone between the belt (Be) and the outer mantle epithelium (OME).* **(H)** *SEM x5330. Fracture face of the shell showing the periostracum (P) and one cross lamellar layer (CLL).* **(I)** *TEM x46120. Section of a decalcified shell. The periostracum has an inner (IL) and outer layer (OL) which might be covered by mucous. The intercrystalline matrix (ICM) consists of osmiophilic envelopes (arrows), which are arranged in one direction. The arrowheads indicate the hypostracum (Hy) which is of medium electron density.*
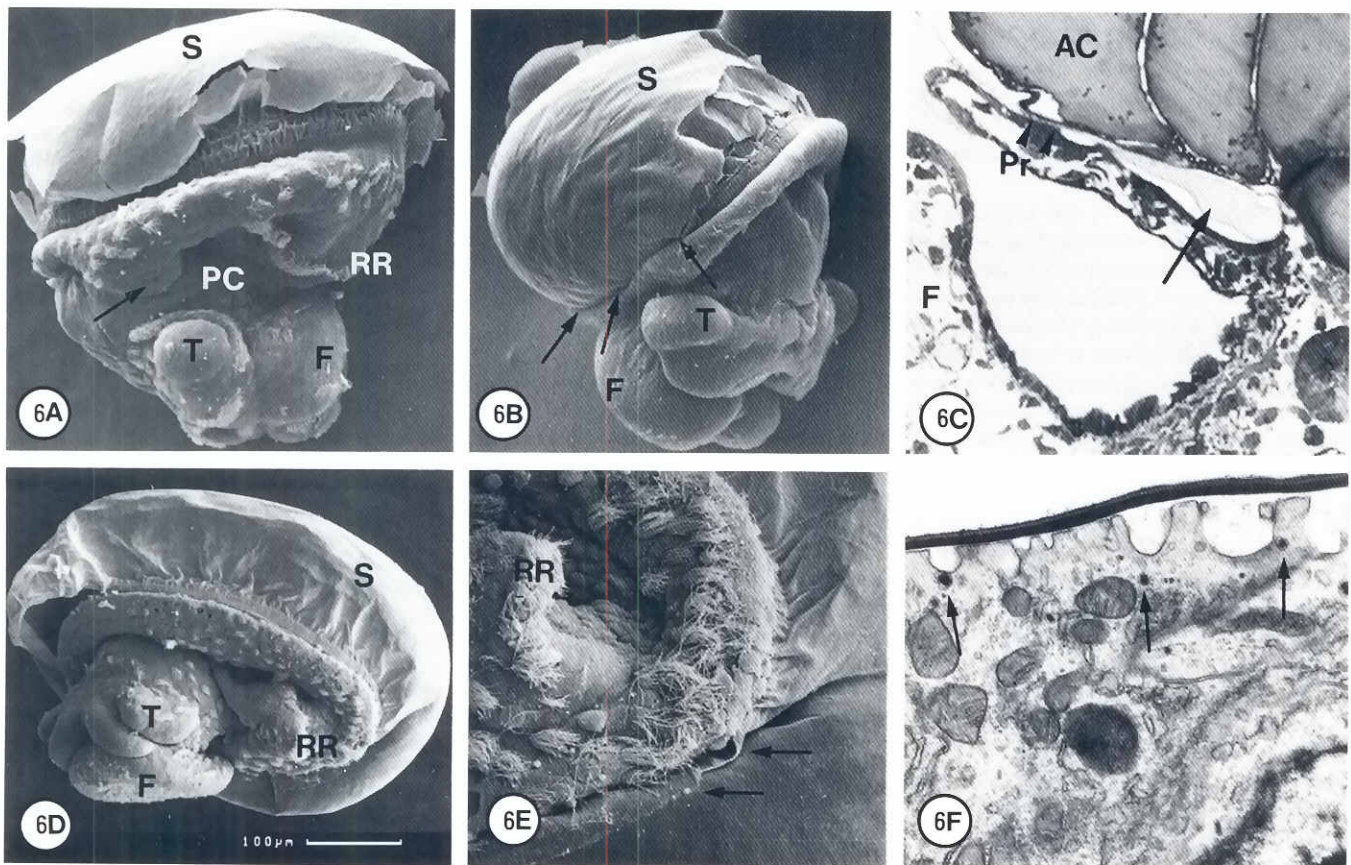
Fig. 6. Spindle formation in veliger stages. (A) *SEM x200. View on the left side of an embryo of 80 h with distinct foot (F), tentacles (T) and calcified shell (S). The pulmonary cavity (PC) extends from the rectal ridge (RR) to the proctodeum (arrrow).* **(B)** *SEM x210. Embryo of 80 h with distinct foot (F), tentacles (T). View on the right side of the embryo. The shell (S) starts to coil at the right and caudal side (arrows).* **(C)** *LM x500. Cross section through an embryo with 80 h of development. At the right side of the body there is a protrusion between the main body indicated by albumen storing cells (AC) and the foot (F). The fold bears shell-secreting cells at the shell facing side (arrowheads). The spindle is indicated by the arrow.* **(D)** *SEM x120. Embryo of 90 h development. View of the left side. At the left side the rectal ridge (RR) protrudes from the pulmonary cavity. Foot (F) tentacles (T) and shell (S).* **(E)** *SEM x360. Ventral view of the closed spindle (arrows) of the same embryo as shown in Fig. 6D. Rectal ridge (RR).* **(F)** *TEM x42930. At the spindle side, the material for the newly-formed periostracum (P) is secreted as electron-dense vesicles (arrows).*

CUMIN, R. (1972). Normentafel zur Organogenese von *Lymnaea stagnalis* (Gastropoda, Pulmonata), mit besonderer Beruecksichtigung der Mitteldarmdruese. *Rev. Suisse Zool. 79*: 709-774.

EYSTER, L. (1983). Ultrastructure of early embryonic shell formation in the opistobranch gastropod *Aeolidia papillosa. Biol. Bull. 165*: 394-408.

EYSTER, L. (1985). Origin, morphology and fate of the nonmineralized shell of *Coryphella salmonacea*, an opistobranch gastropod. *Mar. Biol. 85*: 67-76.

EYSTER, L. (1986). Shell inorganic composition and onset of shell mineralization during bivalve and gastropod embryogenesis. *Biol. Bull. 170*: 211-231.

GOODFORD, P.F. and WOLOWYK, M.W. (1972). Localization of cation interactions in the smooth muscle of the guinea-pig *Taenia coli. J. Physiol. 224*: 521- 535

HOLMES, S.J. (1900). The early development of *Planorbis. J. Morphol. 16*: 369-458.

HUMBERT, W. VOEGEL, J.C., KIRSCH R. and SIMMONEAUX, V. (1989). Role of intestinal mucus in crystal biogenesis: an electron-microscopical, diffraction and X-ray microanalytical study. *Cell. Tissue Res. 255*: 575-583.

JONES, G.M. and SALEUDDIN, A.S.M. (1978). Cellular mechanisms of periostracum formation in *Physa ssp* (Mollusca: Pulmonata). *Can. J. Zool. 56*: 2299-2311.

KAPUR, S.P. and GIBSON, M.A. (1967). A histological study of the development of the mantle edge and shell of the fresh-water gastropod, *Helisoma duryi eudiscus. Can. J. Zool. 45*: 1169-1181.

KARNOVSKY, M.J. (1961). Use of ferricyanide-reduced osmium tetroxide in electron microscopy. *J. Cell Biol. 51*: 284.

KAWANO, T. and SIMOES, L.C.G. (1987): Morphogenetic effects of caffein on *Biomphalaria glabrata* (Pulmonata, Planorbidae). *Proc. Konij. Ned. Akad. Wet. C 90*: 281-304.

KNIPRATH, E. (1972). Formation and structure of the periostracum in *Lymnaea stagnalis. Calcif. Tissue Res. 9*: 260-271.

KNIPRATH, E. (1977). Zur Ontogenese des Schalenfeldes von *Lymnaea stagnalis. Roux Arch. Dev. Biol. 181*: 11-30.

KNIPRATH, E. (1981). Ontogeny of the molluscan shell field: a review. *Zool. Scr. 10*: 61-79.

MCDONALD, K. (1984). Osmiumferricyanide fixation improves microfilament preservation and membrane visualization in a variety of animal cell types. *J Ultrastruct. Res. 86*: 107-118.

MOOR, B. (1983). Organogenesis. In *The Mollusca*, Vol. 3, Development (Eds. N.H. Verdonk, J.A.M. van den Biggelaar and A.S. Tompa). Academic Press, New York. pp. 123- 177.

MORRILL, J. B. (1982). Development of the pulmonate gastropod, *Lymnaea*. In *Developmental Biology of Freshwater Invertebrates* (Eds. F.W. Harrison and R.R. Cowden). Alan Liss, New York. pp. 399- 463.

NAKAHARA, H., KAKEI, M. and BEVELANDER G. (1981). Studies on the formation of the crossed lamellar structure in the shell of *Strobus gigas*. *Veliger 23:* 207- 211.

NEFF, J.M. (1972). Ultrastructural studies of periostracum formation in the hard shelled clam *Mercenaria mercenaria* (L). *Tissue Cell 4:* 311-326.

PROBST, W. (1986). Ultrastuctural localization of calcium in the CNS of vertebrates. *Histochemistry 85:* 231-239.

RABL, C. (1879). Über die Entwicklung der Tellerschnecke. *Gegenbaurs Morphol. Jahrb. 5:* 562- 660.

RAVEN, C.P. (1966). *Morphogenesis. The Analysis of Molluscan Development.* Vol 2. Pergamon Press, Oxford.

RAVEN, C. P. (1952). Morphogenesis in *Lymnaea* stagnalis and its disturbance by lithium. *J. Exp. Zool. 121:* 1-72.

REYNOLDS, E. (1963). The use of lead citrate at high pH as an electron opaque stain in electron microscopy. *J. Cell Biol. 17:* 208-212.

RICHARDSON, K.C., JARRETT, L. and FINKE, E.H. (1960). Embedding in epoxy resins for ultrathin sectioning in electron microscopy. *Stain Technol. 35:* 313-325.

SALEUDDIN, A.S.M. and PETIT, H.P. (1983). The mode of formation and the structure of the periostracum. In *The Mollusca*, Volume 4, Physiology Part I. (Eds. A.S.M. Saleuddin and K.M. Wilbur). Academic Press, New York, pp. 199-234.

SPURR, H. (1969). A low viscosity epoxy resin embedding medium for electron microscopy. *J. Ultrastruct. Res. 26:* 31-41.

STEEN van der, W. J. (1967). The influence of environmental factors on the oviposition of *Lymnaea stagnalis* (L.) under laboratory conditions. *Arch. Neerl. Zool. 17:* 403-468.

TAYLOR H.H. (1973). The ionic properties of the capsular fluid bathing embryos of *Lymnaea stagnalis* and *Biomphalaria sudanica* (Mollusca, Pulmonata). *J. Exp. Biol. 59:* 543-564.

TIMMERMANS, L.P.M. (1969). Studies on shell formation in molluscs. *Neth. J. Zool. 19:* 417- 523.

TOMLINSON, S. G. (1987). Intermediate stages in the embryonic development of the gastropod *Ilyanassa obsoleta:* a scanning electron microscope study. *Int. J. Invert. Reprod. Dev. 12:* 253-280.

VERDONK, N. H. and BIGGELAAR, J. A. M. (1983). Early development and the formation of the germ layers. In *The Mollusca*, Vol. 3, Development (Eds N.H. Verdonk, J.A.M. van den Biggelaar and A.S. Tompa). Academic Press, New York, pp 91-122.

WATABE, N. (1988). Shell structure. In *The Mollusca*, Vol. 11, Form and Function (Eds. E.R. Trueman and M.R. Clarke). Academic Press, San Diego, pp. 69-101.

WIERZEJSKI, A. (1905). Embryologie von Physa fontinalis. *Z. Wiss. Zool. 83:* 502-706.

WILBUR, K.M. and SALEUDDIN, A.S.M (1983). Shell formation.In *The Mollusca*, Vol. 4, Physiology Part I (Eds. A.S.M. Saleuddin and K.M. Wilbur). Academic Press, New York, pp 235-287.

ZYLSTRA, U., BOER, H. H. and SMINIA,T. (1978). Ultrastructure, histology and innervation of the mantle edge of the freshwater pulmonate snail *Lymnaea stagnalis* and *Biomphalaria pfeifferi*. *Calc. Tissue Res. 26:* 271- 282.